Martí Calatayud, MC.; Schneider, S.; Yüce, S.; Wessling, M. (2018). Interplay between physical cleaning, membrane pore size and fluid rheology during the evolution of fouling in membrane bioreactors. Water Research. 147:393-402. https://doi.org/10.1016/j.watres.2018.10.017

Interplay between physical cleaning, membrane pore size and fluid rheology during the evolution of fouling in membrane bioreactors

M.C. Martí-Calatayud[a,b], S. Schneider[b], S. Yüce[b], M. Wessling[b,c,*]

[a] *Universitat Politècnica de València, IEC Group, Departament d'Enginyeria Quimica i Nuclear, Camí de Vera s/n, 46022, València, Spain*
[b] *RWTH Aachen University, Chemical Process Engineering, Forckenbeckstr. 51, 52074 Aachen, Germany*
[c] *DWI Interactive Materials Research, Forckenbeckstr. 50, 52074 Aachen, Germany*

Abstract

Fouling is one of the most pressing limitations during operation of membrane bioreactors, as it increases operating costs and is the cause of short membrane lifespans. Conducting effective physical cleanings is thus essential for keeping membrane operation above viable performance limits. The nature of organic foulants present in the sludge and the membrane properties are among the most influential factors determining fouling development and thus, efficiency of fouling mitigation approaches. The role of other factors like sludge viscosity on fouling is still unclear, given that contradictory effects have been reported in the literature. In the present study we use a new research approach by which the complex interplay between fouling type, levels of permeate flux, membrane material and feed properties is analyzed, and the influence of these factors on critical flux and membrane permeability is evaluated. A variety of systems including activated sludge and model solutions with distinct rheological behavior has been investigated for two membranes differing in pore size distribution. We present a novel method for assessing the efficiency of fouling removal by backwash and compare it with the efficiency achieved by means of relaxation. Results obtained have proven that backwash delays development of critical fouling as compared with relaxation and reduces fouling irreversibility regardless of fluid rheology. It was shown that backwash is especially effective for membranes for which internal fouling is the main cause of loss in permeability. Nonetheless, we found out that for membranes with tight pores, both relaxation and backwash are equally effective. The critical flux decreases significantly for

high-viscosity fluids, such as activated sludge. This effect is mainly caused by an intensified concentration polarization at the feed side rather than by internal fouling events. However, membrane permeability has been proven to rely more on the permeate viscosity than on the feed viscosity: poor rejection of organic fractions showcasing high viscosity causes an acute decline in membrane permeability as a consequence of increased shear stress inside the membrane pores.

Keywords: backwash, membrane bioreactors, physical cleaning, fouling mitigation, relaxation, sludge rheology

---

Nomenclature

BSA	bovine serum albumin	SEM	scanning electron microscopy
BWSM	backwash step method	SWW	synthetic wastewater
CFSM	conventional flux step method	TMP	transmembrane pressure
EPS	extracellular polymeric substances	$\dot{\gamma}$	shear rate
		κ	flow consistency
HPLC	high performance liquid chromatography	τ	shear stress
		τ_0	yield stress
HV-SWW	high-viscosity synthetic wastewater	j_P	permeate flux
		$j_{BW,max}$	maximum backwash flux of the backwash step method
IFSM	improved flux step method		
MBR	Membrane bioreactor	j_{BW}	backwash flux
MLSS	mixed liquor suspended solids	$j_{cr,irr}$	critical flux for irreversibility
MWCO	molecular weight cut-off	j_{cr}	critical flux
PES	Polyethersulfone	$j_{P,max}$	maximum permeate flux of the flux step method
SEC	size exclusion chromatography		

*I am corresponding author
Email addresses: mamarc13@upvnet.upv.es (M.C. Martí-Calatayud), manuscripts.cvt@avt.rwth-aachen.de (M. Wessling)

$L_{p,BW}$	Permeability obtained from the backwash step method at undercritical fluxes	n	cross rate constant
		w_F	weight fraction of dextrans in the feed
$L_{p,IFSM}$	Permeability obtained from the improved flux step method at undercritical fluxes	w_P	weight fraction of dextrans in the permeate

1. Introduction

The integration of membrane separation units with the biochemical degradation of pollutants in membrane bioreactors (MBRs) makes feasible operating wastewater treatment systems at high biomass concentrations. This is done without compromising the effluent quality owing to the high solid/liquid separation efficiency yielded by the membranes. MBR technology is particularly appropriate for the implementation of water reuse schemes in areas of acute water stress. The advantages of MBRs compared to conventional activated sludge processes, such as their robust performance, high effluent quality and reduced footprint (Holloway et al. (2015); Meng et al. (2017)); together with the progress achieved in this field during the last years have contributed to expand their implementation. Nonetheless, membrane fouling is an unavoidable outcome of membrane filtration that still poses to be the most serious challenge in MBRs, as it ultimately entails an increase in operating costs (Zhang et al. (2014)).

The accumulation of matter on the membrane surface and inside the porous membrane network results in increased transmembrane pressures (TMP) and/or decreased permeate fluxes (j_P), thus diminishing the specific process throughput. A critical fouling phenomenon is the manifestation of an acute TMP jump when a specific permeate flux, usually called critical flux (j_{cr}), is surpassed or when MBR systems are operated at demanding conditions for long periods. Fouling in immersed MBRs is caused by different types of species, i.e. inorganic compounds, microbial flocs or organic molecules. Among them, extracellular polymeric substances (EPS) are considered to be one of the major fouling initiators. EPS is a term which comprises organic macromolecules that are released by microorganisms includ-

ing mainly polysaccharides and proteins, but also other compounds such as nucleic acids and lipids (Lin et al. (2014)). EPS show a three-dimensional gelatinous matrix, which provides cell-to-cell scaffolding (Bar-Zeev et al. (2015)). Gel layers can seriously compromise the operability of MBRs, especially when aggravated by interactions taking place with inorganic foulants (Wei et al. (2011)). Besides the nature of the foulants, operating conditions and membrane properties have a crucial impact on fouling development in immersed membrane filtration. Diverse studies have found correlations between fouling propensity and membrane properties, such as hydrophilicity, roughness or pore size (Hashino et al. (2011); Kochkodan and Hilal (2015); Meng et al. (2017)).

As evident from the above discussion, fouling mitigation strategies in MBR systems are indispensable. They are usually classified into (a) physical and (b) chemical cleaning. The former implies the utilization of relaxation and backwash procedures which are able to effectively remove gross solids attached to the membrane and even detach loosely formed cake. The latter involves the use of chemical reagents in order to remove the physically irreversible fouling, which refers to fouling that cannot be removed by using physical cleaning (Wang et al. (2014)). The two prevailing chemicals used are sodium hypochlorite for the organic fouling, and citric acid for the inorganic fouling. These chemicals attack the interactions between the different foulants, as well as between the foulants and the membrane. Although chemical cleaning has proven to be a highly effective method for fouling removal, its frequency should ideally be limited to a minimum level as, when applied repeatedly, it reduces the lifespan of the membranes (Le-Clech et al. (2006); Meng et al. (2009)). Accordingly, physical cleaning is usually preferred, as it does not imply chemical degradation of membranes and can be implemented more frequently. Both relaxation and backwash have been extensively applied to hollow fiber membranes, where backwash has been demonstrated to be more effective in keeping low irreversible fouling rates (Zsirai et al. (2012)). Yet, the application of backwash is not as practical for polymeric flat sheet membranes, as it can induce delamination of the active layers or membrane detachment from the panels (Le-Clech et al. (2006); Wang et al. (2014)). Nevertheless, backwashable flat sheet membranes with enhanced mechanical integrity have recently been introduced. Such membranes are

based on pocket configurations or on the integration of spacer fabrics between two flat sheet membranes (Doyen et al. (2010); Wang et al. (2014)).

Fouling phenomena are commonly investigated by utilizing flux-stepping protocols, which serve for assessing the evolution of permeability at different flux levels and for determining critical permeate fluxes. The simplest flux-stepping method, called here conventional flux step method (CFSM), is based on filtrating during short periods with stepwise increments of the flux level. The TMP transients, induced by an increased deposition of foulants occurring after each step transition, are then evaluated. Van der Marel et al. modified the CFSM by introducing relaxation steps between each flux increase (van der Marel et al. (2009)). In such a way, they calculated critical fluxes with intercalated physical cleanings, as it is usually practiced in MBRs. Additionally, the permeability of the membranes measured after each cleaning step allows calculating the critical flux for irreversibility ($j_{cr,irr}$), which is defined as the flux at which fouling cannot be removed by intermediate physical cleanings. They coined this method with the term 'improved flux-step method', or shortly, IFSM. The efficiency of the intermediate physical cleaning may, however, vary depending on the cleaning procedure applied. In this vein, backwash is expected to be more effective in removing cohesive fouling than relaxation, although at the expense of reducing water production rates. Nevertheless, there is no clear knowledge about to which extent backwash is more effective than relaxation and whether there are specific cases where one of both physical cleanings is preferred. Comparison of efficiency of both physical cleaning methods in flat-sheet membranes is necessary in order to find optimum operating conditions for MBRs.

The peculiar rheology of biological activated sludge increases complexity of fouling in MBRs. Activated sludge is usually highly viscous due to the presence of biological flocs, EPS and suspended solids. This effect is even intensified in the case of MBR sludge, owing to its high concentration in mixed liquor suspended solids (MLSS). High viscosities may turn into considerably high energy costs because of higher demands of aeration for both oxygen transfer and membrane scouring as well as for permeate pumping (Laera et al. (2007)). On the one hand, as solution viscosity varies within diffusion boundary layers, a high viscosity is expected at the membrane surface, thus intensifying concentration polarization and

decreasing mass transfer rates (Charcosset and Choplin (1995)). On the other hand, activated sludge is also known to exhibit shear-thinning properties (Rosenberger et al. (2016)). Pritchard et al. observed that an increase in bulk viscosity during the ultrafiltration of a non-Newtonian fluid caused an increase in permeate flux. This effect was attributed to the maximum shear stress taking place at the membrane surface, implying lower viscosities at the membrane interface when shear-thinning fluids are filtrated (Howell et al. (1996); Pritchard et al. (1995)).

In view of the complexity of fouling processes in MBRs, the present work aims to provide a systematic approach to characterize fouling occurring in immersed flat-sheet membranes by considering interactions between fluid rheology, membrane pore sizes and physical cleaning procedures. A special emphasis is given to effects of backwash filtration on the development of critical fouling phenomena. To this end, for the first time a novel flux-step method including intermediate backwash steps is developed and compared to the IFSM procedure. Effects on hydraulic resistance, critical flux, and irreversibility of fouling are assessed for membranes with different pore size distributions and for a variety of solutions having Newtonian and non-Newtonian behavior. In consequence, the principal objective of this work is to identify interactions between different process parameters, which are relevant for fouling development in MBRs. Given the variety and often contradictory conclusions drawn from different studies across the literature (Drews (2010)), we aim at providing a clear interpretation to the correlation between these parameters and their influence on the performance of immersed MBRs.

2. Experimental

2.1. Materials

Two different commercial ultrafiltration membranes were selected for conducting the present study: the membrane UP150 (Microdyn Nadir, Germany), from here on referred to as UP, and the membrane LY100 (Synder Filtration, United States), referred as LY. The active layer of both membranes is made of polyethersulfone (PES), while the backing

material is polypropylene for UP and polyester for LY. The UP membrane has a molecular weight cut-off (MWCO) specification of 150 kDa, whereas the LY has a MWCO of 100 kDa. The contact angle at the active layer is 55.86 ± 3.27 for UP and 72.72 ± 3.29 for LY.

A synthetic model wastewater (SWW) resembling the typical composition of wastewater was selected for the present investigation. The type of compounds and their concentrations were selected based on previous studies (Xing et al. (2010); Zhang et al. (2013)). Sodium alginate (50 mg/l), glucose (100 mg/l) and BSA (10 mg/l) were selected as typical polysaccharides and proteins, respectively; which are also the most typical model foulants for EPS. Sodium bicarbonate (100 mg/l), magnesium sulfate (30 mg/l) and calcium chloride (111 mg/l) were selected in order to set constant ionic environment for all experiments. For the sake of comparison, other solutions with different rheological behavior were also investigated. The same compounds and concentrations were used with a 30%v/v glycerin/water mixture (high-viscosity wastewater, HV-SWW) with the aim of simulating fouling under viscosity conditions close to those found in MBR sludges. Finally, the results were also contrasted with activated sludge taken from a real MBR treating wastewaters generated in the food industry. The sludge had a MLSS concentration of 15 g/l, and the MBR was operated with a sludge retention time of approximately 28 days. In order to ensure constant conditions of the sludge samples throughout the experiments and to avoid further microbial growth as well as degradation of potential foulants, sodium azide (NaN_3) was added to the samples with a concentration of 0.02%w/w. Additionally, the samples were stored at a temperature below 5°C.

2.2. Setups and procedures

The rheological behavior of the three different samples was obtained using a rheometer MCR 102 (Anton Paar) with a double gap cylinder (DG42) measuring system at a controlled temperature of 25°C. This type of measurement system is composed of a concentric cylinder, which has relatively larger surface areas and lower gap distances as compared to other measuring systems. This makes double gap cylinders more appropriate for liquids with low viscosities and avoids the early onset of turbulences at low shear rates. Flow curves ranging

from shear rates of 1 s^{-1} up to 2000 s^{-1} were registered. Chromatographic measurements of pre-filtered MBR sludge were performed in order to obtain the molecular characterization of different compounds present in it. Additionally, the feed wastewater and MBR permeate were also analyzed. These samples were vacuum filtered to remove suspended solids employing a regenerated cellulose filter with a pore size of 0.45 μm. The different samples were injected in volumes from 20 μl to 100 μl in a HPLC 1100 instrument (Agilent), applying a flow rate of 1 ml/min. The separation was performed using the columns Suprema 10 μm and Suprema 30 A 10 μm (from Polymer Standards Service GmbH). The detection was carried out utilizing a diode array detector at a wavelength of 254 nm in combination with a refractive index detector. In order to calibrate the molecular weight distribution with the elution volume times, different dextran standards were injected and analyzed (having peak maximums corresponding to the following molecular weights: 180, 342, 1080, 4400, 9900, 21400, 124000 and 401000 Da).

A preliminary characterization of the membrane structure was conducted for both membranes. Scanning Electron Microscopy (SEM) images of both membranes were taken, and pore size characterization was conducted by means of MWCO measurements. For the MWCO measurements, a stirred dead-end filtration unit was used at a TMP of 0.5 bar. The solution filtered was a mixture of different dextran standards with a total concentration of 2.5 g/l (0.5 g/l dextran 40 kDa, 1 g/l dextran 100 kDa and 1 g/l dextran 500 kDa). The concentrations of dextrans of different molecular weight in feed and permeate were determined by size exclusion chromatography (SEC) using a refractive index detector. Dextrans have different affinity to the column depending on their molecular weight, so that the evolution of the strength of the refractive index signal provides the molecular weight distribution of the different samples. Accordingly, the rejection curves can be obtained by calculating $1 - w_P/w_F$ for each molecular weight, where w_P and w_F represent the mass fraction of dextrans in permeate and feed, respectively. The $MWCO_{90}$, which corresponds to a 90% of solute rejection, was then calculated for both membranes.

The membrane filtration experiments were conducted using a setup described in detail in a previous publication (Martí-Calatayud and Wessling (2017)), in which a panel with two

flat sheet membranes clamped at both its sides was immersed into the reactor and it was aerated via two blowers placed below the filtration module. The permeate was extracted via a peristaltic pump (Ismatec Reglo), the speed of which was regulated and automated using a data logger and control system based on the software DasyLab. The pressure at the permeate side was measured by using a pressure sensor (Wika Type D-10, Wika), and was registered in order to calculate the TMP by means of the following equation:

$$TMP = p_{feed} - p_{permeate} \tag{1}$$

Where p_{feed} was taken as the atmospheric pressure. The aeration in the membrane reactor was supplied by an air compressor (AquaForte V60). The aeration flow was set constant at 1 L/min. The volume capacity of the reactor is 3.3 L, and the effective membrane area was 126 cm^2.

Fig. 1 shows comparison between the so-called improved flux step method, IFSM, introduced by Van der Marel et al. (van der Marel et al. (2009)), and the novel backwash step method (BWSM), designed and implemented for the first time in the present article. As mentioned above, the permeate flux, j_P, in the CFSM is increased step-wise until the maximum is reached, and then decreased again in a descending phase. The IFSM (Fig. 1(a)) includes a relaxation step after each filtration period and prior to implementing a subsequent flux increase. Here, it is to be noted that the relaxation step is not a complete cessation of filtration, but an intermediate filtration step at a very low flux, where aeration is maintained. In the present work, we introduce a new method for characterizing membrane filtration with intermediate backwash cleaning. As can be seen in Fig. 1(b), at the start of the filtration function the flux is small. So it is impractical to apply very high backwash fluxes and consume more permeate than that produced during the previous filtration. In such case, a compromise between backwash duration and intensity was found, where the backwash was selected to be half of the previous filtration flux:

$$j_{BW} = \frac{j_P}{2} \tag{2}$$

Within the central part of the BWSM function, a standard maximum backwash flux

$j_{BW,max}$ was implemented. The selected value along with the backwash duration (2 min) was optimized during preliminary experiments so as to ensure effective membrane cleaning.

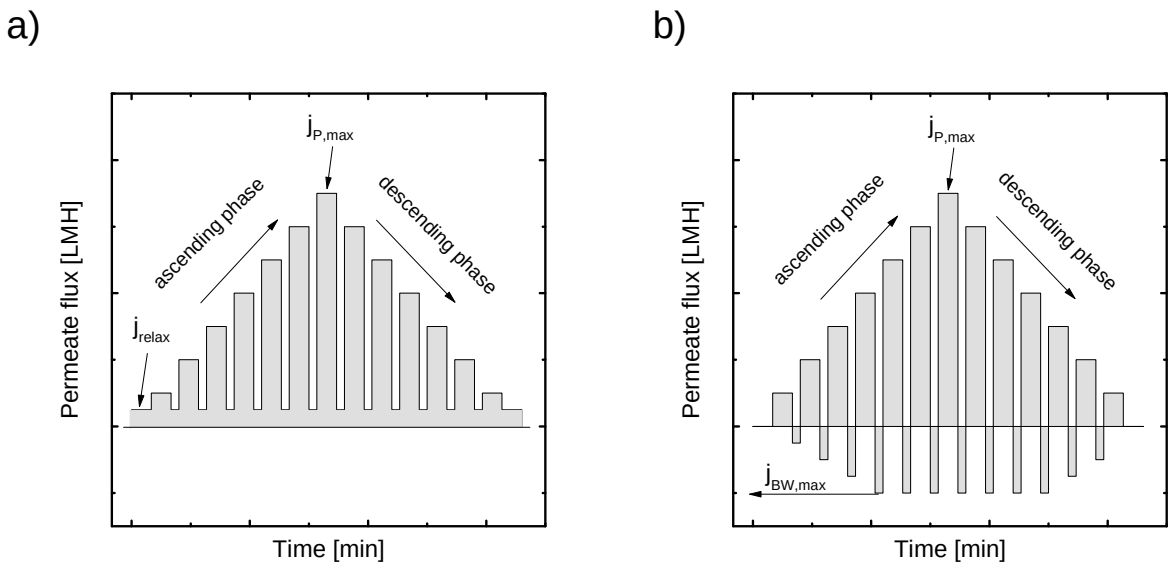

Figure 1: Schematic representation of the input function applied for (a) the IFSM and (b) the BWSM.

An additional feature common to the flux step methods implemented in the present work is that all of them count with an uprising phase where the flux is gradually increased, and a symmetrical descending phase, which is used in order to identify hysteresis phenomena indicative of irreversible fouling. The conduction of IFSM and BWSM is used in order to identify changes in membrane permeability after different types of physical cleaning for a wide range of operating fluxes. The filtration steps were increased by 5 LMH until they reached a maximum flux $j_{P,max}$ slightly above 100 LMH, for the experiments conducted with SWW. Due to the higher viscosity of MBR sludge and HV-SWW, the maximum flux was set to 30 LMH for these solutions and the step increase was selected to be 2.5 LMH.

3. Results

3.1. Rheology of used solutions and membrane characterization

The viscosity of MBR activated sludge and of SWW were measured in order to check the disparity between the samples. Subsequently, the viscosity of the sludge was taken as a reference in order to prepare HV-SWW. The viscosity at high shear rates of 1000 s^{-1} (0.0032 Pa·s) was considered to determine the proportion of glycerin to be used and prepare HV-SWW based on the formulas provided by Cheng for water-glycerin mixtures (Cheng (2008)). Fig. 2 shows the dependency of viscosity on shear rate for the three solutions considered. In line with the rheological calculations of sludge samples reported in previous studies (Rosenberger et al. (2016)), the MBR activated sludge clearly shows shear-thinning properties, since viscosity significantly decreases at increasing shear rates. The viscosity of SWW at high shear rates (1000 s^{-1}), 0.00109 Pa·s, is close to that of water, hence, indicating that addition of foulants does not significantly alter the solution viscosity in this range of shear rates. However, the addition of foulants imparts non-Newtonian behavior to the mixture. The dependency of viscosity on shear rates is very similar to that observed for the sludge. Here it must be mentioned that the increase in viscosity observed for higher shear rates ($>>$ 1000 s^{-1}) is caused by Taylor vortices occurring in the rheometer, which should not be taken into account (Ratkovich et al. (2013)). The viscosity of HV-SWW solutions at a shear rate of 1000 s^{-1} (prepared with 30% v/v glycerin) practically coincides, as expected, with that of the sludge; however, their rheological behavior notably differs from that of SWW and MBR sludge. HV-SWW basically showcases a Newtonian behavior and it only shows noticeable variations at shear rates lower than 10 s^{-1}. The rheogram of Fig. 2(b) confirms these observations: MBR sludge and SWW exhibit an attenuating increase in shear stress at increasing shear rates; on the contrary, HV-SWW shows a linear trend. The rheograms were fitted to the Herschel-Bulkley model commonly used for modeling activated sludge rheology (Rosenberger et al. (2016)).

$$\tau = \tau_0 + k \cdot \dot{\gamma}^n \tag{3}$$

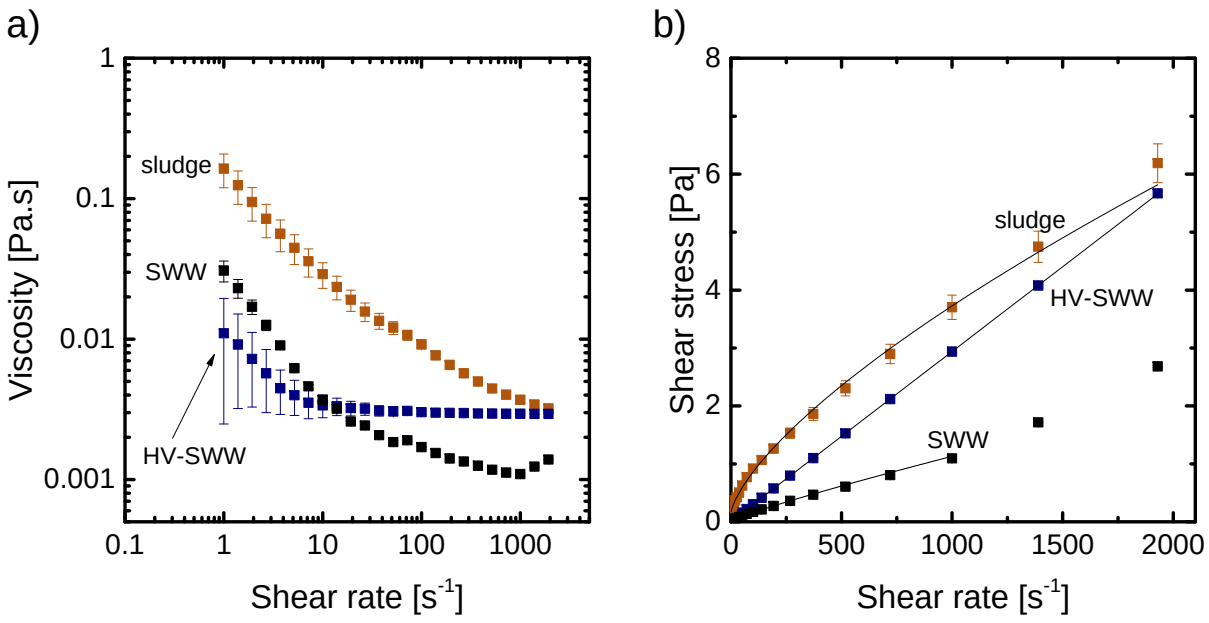

Figure 2: Rheological behavior of the solutions used in the present study: (a) viscosity as a function of shear rate and (b) shear stress as a function of shear rate at a temperature of 25° C.

where τ represents the shear stress ($Pa \cdot s$), τ_0 the yield stress (Pa), k the flow consistency index ($Pa \cdot s^n$) and n the cross rate constant. The exponent n takes values lower than 1 for shear-thinning fluids, 1 for Newtonian fluids and higher values for shear-thickening fluids. The fittings obtained for MBR sludge and SWW were $\tau = 0.144 + 0.028 \cdot \dot{\gamma}^{0.69}$ and $\tau = 0.018 + 0.002 \cdot \dot{\gamma}^{0.89}$, respectively. Consequently, the cross rate constants of 0.69 for MBR sludge and 0.89 for SWW corroborate their non-Newtonian properties. On the contrary, the rheological behavior of HV-SWW could be fitted with the power law function $\tau = 0.003 \cdot \dot{\gamma}^{0.99}$, which confirms its Newtonian properties.

Regarding the membrane characterization, SEC retention curves calculated for both membranes are presented in Fig. 3(a). The experimental MWCO values determined were 186 kDa and 1615 kDa for the LY and UP membrane, respectively. This difference implies a significant disparity between the pore sizes of both membranes. In addition to this, the range of pore sizes of the UP membrane is significantly broader, as it encloses values from around 1 kDa to above 10^4 kDa. SEM pictures of the surface of both membranes also

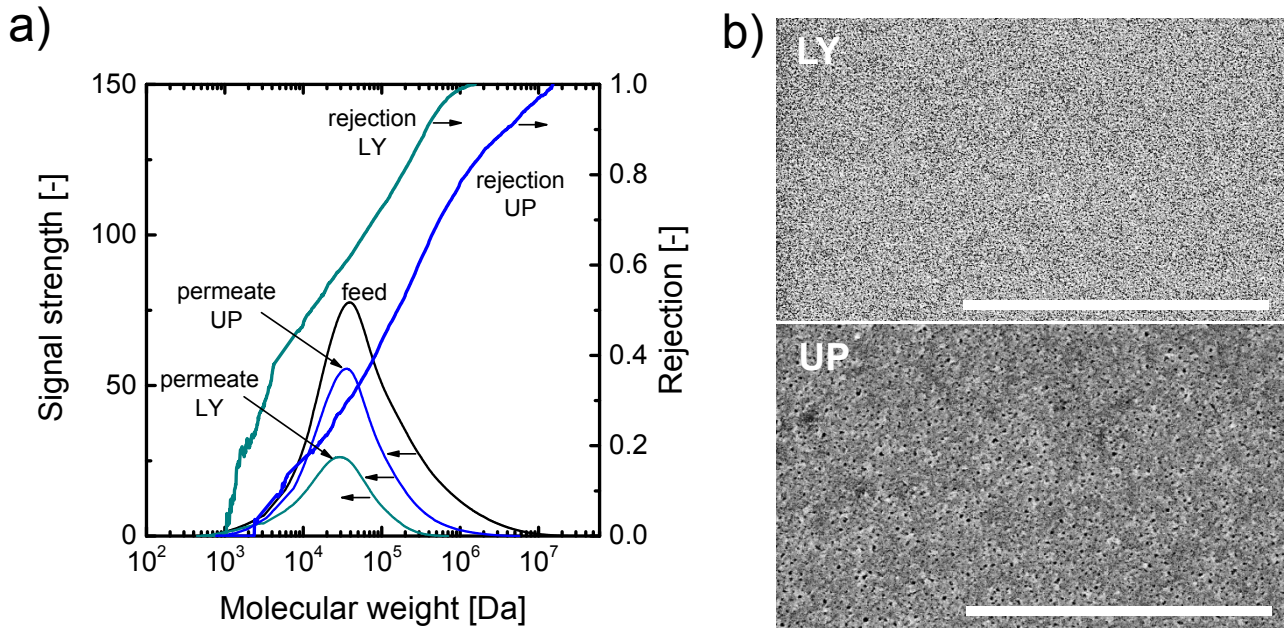

Figure 3: Characterization of UP and LY membranes: (a) SEC characterization for the determination of the MWCO and (b) SEM pictures of the surface of both membranes. The white bar at the bottom of the pictures indicates a length of 2 μm

illustrate substantial differences regarding the pore sizes. LY pores are very difficult to be seen in the picture due to their small width, while the active layer of UP has larger pores and, in general, less uniform pore sizes throughout the membrane surface. Lower porosity of the LY membrane can also be inferred from the pictures.

3.2. Fouling tests with the improved flux-step method

Fig. 4 shows one of the results obtained after applying the IFSM procedure for SWW solutions. Schematic determinations of the critical flux (j_{cr}) and the critical flux for irreversibility ($j_{cr,irr}$) are included in the graph. TMP increases during the filtration steps with different slopes depending on the level of permeate flux. In the ascending phase, at low fluxes a steady TMP value is reached, whereas at higher fluxes the TMP increase is more acute. Drawing two lines connecting the last TMP values registered during the filtration steps at low and high fluxes allows us to calculate an approximate estimation of the j_{cr},

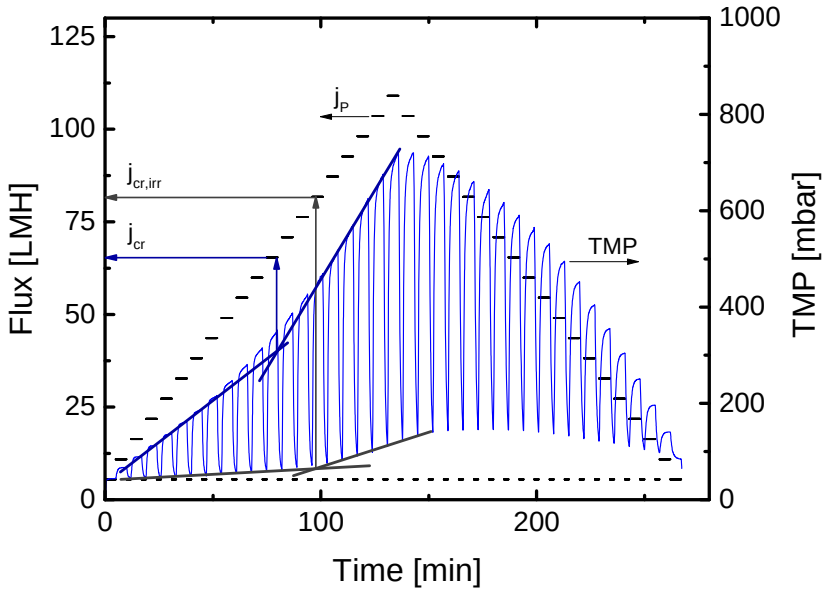

Figure 4: Example of an IFSM experiment conducted with SWW and LY membranes.

which in the example figure takes a value of 65 LMH. The response in the descending part of the graph shows a significant asymmetry compared to the ascending part, which gives an indication of cohesive fouling occurring during the experiment. Thus, membrane permeability cannot be restored to its initial values just by decreasing flux. An additional feature of the IFSM protocol is the profile of TMPs registered during the relaxation steps. Here, also the final TMP values rely strongly on the previously applied flux. At low fluxes, TMP reaches almost the same residual value. However, at fluxes higher than j_{cr} the TMP value remaining before the beginning of new filtration steps increases considerably and does not recover the initial value registered for low fluxes. The trends of TMP during relaxation after applying high and low fluxes were also fitted to visually indicate the calculation of $j_{cr,irr}$. As in van der Marel et al., taking a value of 80 LMH for the case presented in the graph, $j_{cr,irr}$ exceeds j_{cr} significantly (van der Marel et al. (2009)). These results indicate that at fluxes slightly higher than j_{cr}, the development of fouling has a reversible character and thus, can be removed by intermediate relaxation cycles. However, at fluxes higher than $j_{cr,irr}$ the efficacy of relaxation decreases. A possible reason for this difference could be the transition between the deposition of loosely attached fouling and the development of cohesive fouling,

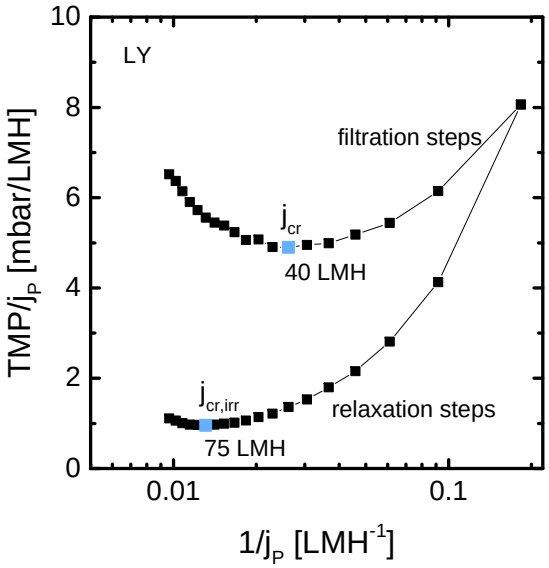

Figure 5: Determination of j_{cr} and $j_{cr,irr}$ from TMP/j_P vs. $1/j_P$ plots. Example corresponding to an IFSM experiment conducted for LY membranes with SWW solutions. Note that only the values corresponding to the ascending phase of the experiment are represented in this plot.

caused by the compression of fouling deposits. The access of foulants to the pores at higher driving forces or the growth of thicker gel layers on the membrane surface could also explain the differences between j_{cr} and $j_{cr,irr}$. Indeed, the formation of a gel layer on the membrane surface was verified at the end of each experiment.

The values of j_{cr} and $j_{cr,irr}$ were calculated accurately by treating the data from the IFSM experiments and representing TMP/j_P against $1/j_P$. These plots are analogous to the Cowan-Brown plots used in electrodialysis for determining limiting currents (Baker (2004); Martí-Calatayud et al. (2013)). Basically, TMP/j_P is proportional to the hydraulic resistance and is represented against the inverse of the permeate flux. After TMP/j_P reaches a minimum, the j_{cr} is exceeded and the resistance of the system grows abruptly. Therefore, the permeate flux corresponding to the minimum in the plots can be used to directly extract the values of j_{cr} and $j_{cr,irr}$ from their respective curves. The same procedure was employed with all membrane systems for all repetitions. The average values of both types of critical flux are summarized in Table 1. The values obtained for both membranes are strongly

Table 1: Values of j_{cr} and $j_{cr,irr}$ obtained for different solutions and membranes from IFSM experiments. All values are given in LMH.

Solution	UP		LY	
	j_{cr}	$j_{cr,irr}$	j_{cr}	$j_{cr,irr}$
SWW	49.1	100.8	41.8	78.2
HV-SWW	11.8	16.3	10.0	20.0
MBR sludge	26.8	>30.0	15.0	25.0

dependent on the type of solution used, while the differences between both membranes are small. Dependency between critical fluxes and solution viscosity can be observed, since the values obtained for SWW are by far the highest. Yet, the values obtained for HV-SWW and MBR sludge differ significantly. On the basis of the rheological properties of the samples alone, these differences were in principle not expected, as both solutions have the same viscosity at high shear rates and the viscosity at low shear rates is even lower for HV-SWW (cf. Fig. 2). Another remarkable fact is that, as exemplified in Fig. 4, in all cases $j_{cr,irr}$ exceeds j_{cr} considerably. Thus, the intermediate regime where fouling develops faster but can still be removed by intermediate relaxation is common to all membrane and solution combinations.

The representation of flux against the last TMP values of each filtration step for all membrane-solution combinations tested are presented in Fig. 6 . Regarding the differences between both membranes, it can be seen that, in general, the permeability of UP is higher than that of LY. These differences are mostly determined by the membrane porosity, although the higher hydrophilicity of UP may also contribute to the higher permeabilities obtained for this membrane. The slight differences in j_{cr} between both membranes seem to be caused also by the differences regarding the size and distribution of pores. The attainment of a sufficiently high local flux at some small pores can boost colloid-colloid interactions and

initiate their coagulation at the pore entrance. Consequently, some parts of the membrane surface become impermeable, and the local flux at the remaining permeable parts intensifies, leading to the strong increase in resistance after exceeding j_{cr}. With the LY membrane, the lower density of pores implies higher local fluxes, hence leading to lower values of j_{cr}.

Besides membrane permeability and critical fluxes, the differences between the ascending and descending phase of IFSM experiments also give an idea of fouling reversibility. The same permeate flux causes higher TMP values at the descending phase due to irreversible fouling deposited during the previous flux steps. Accordingly, the area between the j_P-TMP curves registered in the ascending and descending phases provides an estimation of the irreversible character of fouling taking place during the measurement. In Fig. 6 all curves except for the system UP-sludge exhibit a hysteresis loop indicating that irreversible fouling has occurred during the measurements. Conversely, in the case of UP-sludge, the ascending and descending phases of the IFSM measurement coincide as fouling deposited during each filtration step is removed during the intermediate relaxation. These results are also in agreement with the fact that no $j_{cr,irr}$ could be obtained from the data treatment (see Table 1). As long as $j_{cr,irr}$ is not exceeded, the influence of fouling history is practically absent in the curves.

3.3. Fouling tests with the backwash-step method

The BWSM was implemented for the same solutions and membranes as the IFSM. Fig. 7 shows an example of the evolution of TMP obtained during these experiments. The first observable fact is the almost symmetrical evolution of TMP in the ascending and descending phases, which already gives an idea of the reversible nature of fouling deposited during the experiment. Intermediate backwash steps are able to remove fouling before it turns into irreversible. The TMP evolution during a filtration step is similar to that during normal IFSM experiments; however, the evolution during the backwash is remarkably different. The attainment of negative pressures indicates the effective change of the direction of flux through the membranes, taking place during the physical cleanings. Since the permeate pressure sensor is only able to measure values up to -110 mbar, it was not possible to

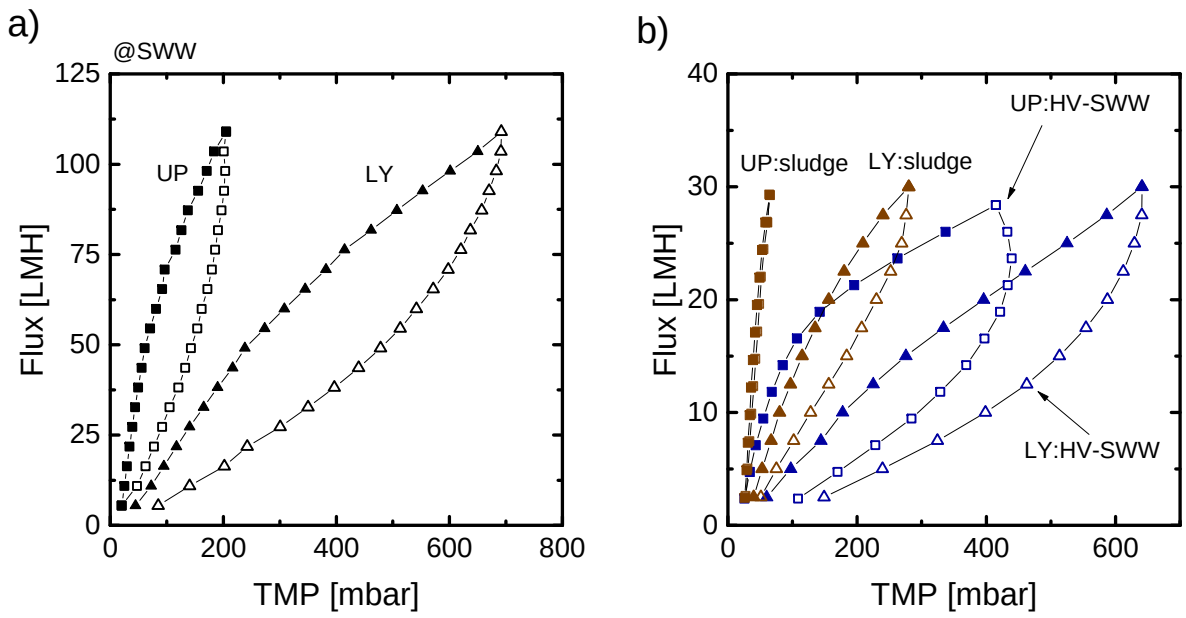

Figure 6: Comparison of the fouling curves obtained from the IFSM measurements for both membranes: (a) Curves obtained using SWW solutions and (b) curves obtained using MBR sludge and HV-SWW solutions. Filled dots represent the values obtained during the ascending phase of the IFSM experiments; empty dots represent those obtained in the descending phase.

register higher TMP values during backwash. As seen from the graph, backwash is mostly effective in removing foulants, since the increase in TMP during a subsequent filtration step is substantially attenuated.

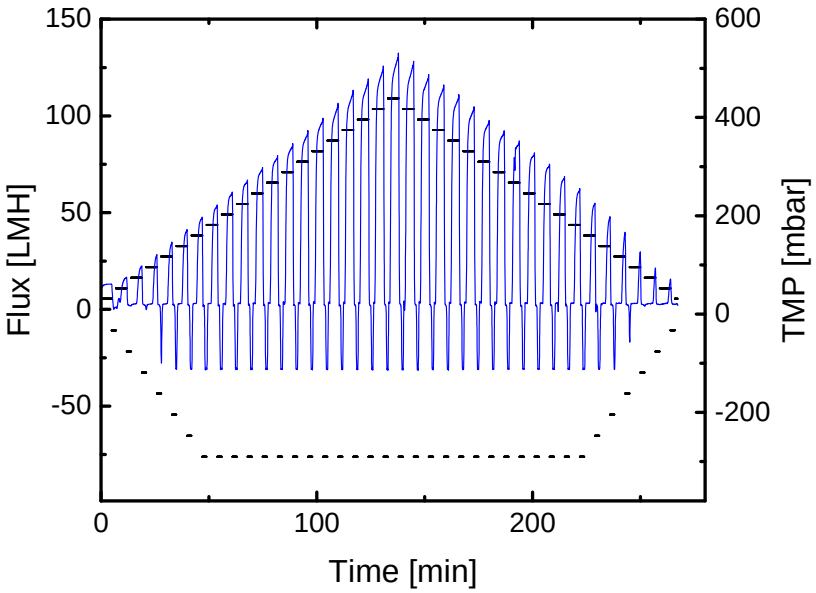

Figure 7: Example of a BWSM experiment conducted with SWW and LY membranes.

Fig. 8 shows a comparison between the fouling curves obtained from IFSM and BWSM experiments with SWW and HV-SWW solutions. All cases show the same behavior: at fluxes below j_{cr}, the curves obtained from both methods are similar; whereas at higher fluxes, the change in permeability for the BWSM curves is very smooth compared to that observed for IFSM, where the increase in membrane resistance is very notorious. Backwash intercalated between filtration steps induces a delay or attenuation of fouling within the range of fluxes tested, which is not achieved by means of relaxation. In view of these results, backwash demonstrated to be capable to remove more cohesive fouling than relaxation, thus preventing or rather postponing the attainment of a j_{cr}. This effect is also evident from the hysteresis observed with IFSM, which is absent in the case of the BWSM.

Despite the apparently similar permeability obtained from both methods at low fluxes, the values calculated indicate substantial differences in some cases, which are not directly observable from the graph due to the used scales. Table 2 summarizes the permeability of

each system with IFSM and BWSM protocols. The values shown are the averages of the different repetitions conducted in each case. As already seen in section 3.2, the permeability of LY is smaller compared to that of UP in all cases. Again, these results correspond with the low density of pores observed for the LY membrane in Fig. 3(b). With regard to the different solutions, the trends follow the decreasing order: SWW > MBR sludge >> HV-SWW. Curiously, the permeability obtained with MBR sludge is close to the one obtained with SWW, although both solutions differ in terms of viscosity significantly.

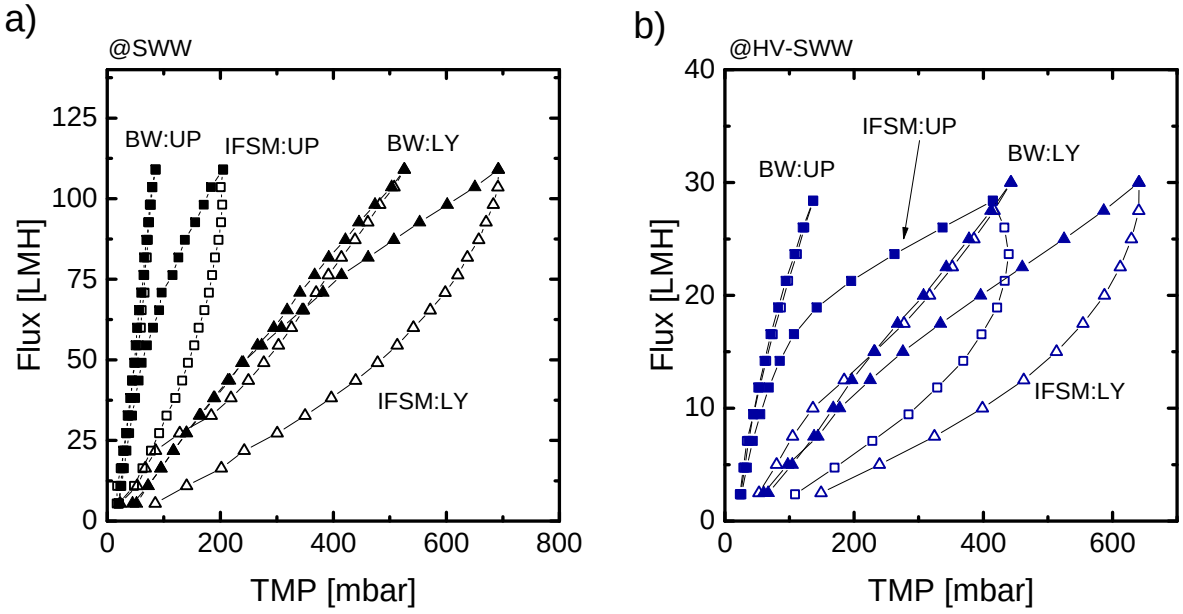

Figure 8: Comparison of the fouling curves obtained from the IFSM and BWSM measurements for both membranes: (a) Curves obtained using SWW solutions and (b) curves obtained using HV-SWW solutions. Filled dots represent the values obtained during the ascending phase of the experiments, while empty dots represent those obtained in the descending phase.

Regarding the differences between membrane permeability obtained with intermediate relaxation and intermediate backwash steps, the performance of the UP membrane seems to be more influenced by the type of physical cleaning. It seems that the UP membrane is more affected by pore clogging even at low permeate fluxes, while LY gets clogged only when high TMP values are applied and foulants get trapped or form a gel layer.

Table 2: Values of permeability obtained at undercritical fluxes from the IFSM experiments ($L_{p,IFSM}$) and BWSM experiments ($L_{p,BW}$) calculated for different solutions and membranes. All values are given in LMH/bar.

Solution	UP		LY	
	$L_{p,IFSM}$	$L_{p,BW}$	$L_{p,IFSM}$	$L_{p,BW}$
SWW	925.7	1415.5	223.1	216.7
HV-SWW	222.9	343.3	61.6	73.2
MBR sludge	831.1	1420.7	176.8	235.2

4. Discussion

The results obtained showed different trends depending on the type of membrane material and on the solution characteristics. A remarkable observation is the low permeability of the LY membrane caused by the low density of pores available for the transport of water. However, this membrane showed low fouling propensity at undercritical fluxes, as revealed by the modest change in permeability when applying intermediate relaxation or backwash. The small pore size of LY makes this membrane less susceptible to pore clogging, as foulants are rejected to a higher extent and their access to the internal membrane structure is hindered. This hindrance is only overcome when high driving forces are applied, concentration polarization is intensified and j_{cr} is attained. Compared to relaxation, the application of backwash at undercritical fluxes does not provide a significant improvement in fouling removal regardless of solution viscosity. Under conditions of low flux and small pore sizes, implementation of relaxation would suffice to remove the loosely attached fouling and backwash would only imply a loss of permeate production. On the contrary, applying of backwash to membranes with a broader pore size distribution, like UP, can be advantageous already at low fluxes, as internal fouling may develop even at low fluxes when solutes and pore sizes are similar. The results obtained are in agreement with the observations of Le Clech et al.:

narrow pore size distributions reduce the inhomogeneous flow distribution between pores that lead to preferential deposition and blockage of membranes with large pores (Le-Clech et al. (2006)).

In the regime of high fluxes, the advantages of using backwash are generalized for both membranes. The values of j_{cr} and $j_{cr,irr}$ calculated with intermediate relaxations do not correspond with the development of critical fouling when physical cleaning is conducted by backwash. In this regard, intermediate backwash is able to suppress or delay the attainment of a critical flux. In addition to this, the curves obtained in the ascending and descending phase of the BWSM experiments are overlapping and verify the lack of hysteresis. Accordingly, a high degree of reversibility of fouling can be ensured by backwash, as the j_P-TMP evolution remains independent of the membrane filtration history. These observations indicate that formation of gel layers may be the main phenomenon originating critical fluxes in the present work. Formation of gel layers, contrary to pore clogging, may evolve similarly for both types of membranes, as it is not as much affected by the pore size.

Unexpected phenomena have also been observed regarding the role of solution viscosity on membrane performance. The permeability of both membranes when filtering MBR sludge is in the same range as for SWW, although the viscosity of the sludge is threefold higher. The viscosity of activated sludge increases with the sludge MLSS and has been attributed a relevant role on causing increased fouling rates (Laera et al. (2007); Rosenberger et al. (2002)). Higher MLSS concentrations are also related to higher production of EPS. In this respect, numerous studies have been conducted to assess effects of viscosity, sludge retention times and MLSS concentration of MBR sludge on membrane fouling and permeability (Meng et al. (2007); Moreau et al. (2009); Wu et al. (2007)). Nonetheless, conclusions drawn across different studies are frequently contradictory. The complexity of sludge matrices makes it especially difficult to extract clear trends from different experimental results. Often some specific sludge properties are the focus of research, while other relevant factors are overlooked. In order to elucidate the reason for the relatively high permeabilites obtained with MBR sludge compared to HV-SWW solutions, a deeper investigation of the fractions present in the MBR sludge was performed. The filtrate of MBR sludge using a filter with pore size

of 0.45 μm was characterized by means of SEC in order to obtain an estimation of the fractions of molecular weights present in the sludge. Fig. 9 shows the molecular characterization of the sludge filtrate, MBR feed wastewater and MBR permeate. Compounds with high molecular weights appear at low elution volumes, while smaller molecules are detected at larger elution volumes. The verticals drawn in the graph correspond to the characteristic peak maximums detected when dextran standards were injected. They serve as a reference to assign certain molecular weights with different elution volumes given the assumption that they interact similarly with the column as the sludge filtrate. Molecular weight bands appearing at elution volumes lower than 6.2 ml thus correspond with high-molecular weight bio-polymers. These compounds are not present in the incoming MBR wastewater so that they are related to biomass growth in the bioreactor. The peak appearing at 7.8-7.9 ml is common to the three samples analyzed, hence it is probably associated with polysaccharides present in the wastewater, and also with EPS with a molecular weight ranging from 350 Da up to 4.4 kDa. Finally, the last peak corresponds to NaN_3 added to the samples in order to prevent microbial growth in the measuring devices.

The chromatograms indicate that the fraction of bio-polymers rejected by the membrane is probably the principal contribution to the high sludge viscosity. In order to corroborate this hypothesis, the viscosities of permeate samples obtained when filtering the three solutions considered were also measured. The values obtained at a shear rate of 1000 s^{-1} were 0.898, 2.502 and 0.903 $mPa \cdot s$ for SWW, HV-SWW and MBR sludge, respectively (detailed graphs of the rheological behavior of different permeates can be found in the Appendix). These results confirm that the viscosity of MBR sludge permeate is very close to that obtained for SWW, which is in agreement with the similar permeability obtained for both solutions. Conversely, the viscosity of HV-SWW permeate is very close to that of the original HV-SWW (3.2 $mPa \cdot s$). Consequently, the transport of permeate through the membrane pores seems to be the phenomenon inducing a low permeability in the case of HV-SWW. Effects caused by MBR sludge viscosity are, conversely, only relevant at the membrane feed side. If the viscosity of the corresponding permeate is used to calculate the membrane hydraulic resistance from the permeability reported in Table 2, the values

obtained for the different solutions become quite similar. The role of fluid flow resistance inside the membrane porous network and the relevance of membrane selective properties on MBR performance has not been given special attention in the literature. In this regard, it is important to mention that Rosenberger et al. already highlighted the importance of the sludge organic liquid fractions on membrane fouling (Rosenberger et al. (2016)). Nonetheless, the role of permeate viscosity was not treated in detail. Using a different approach, Moreau et al. reviewed the effects of sludge viscosity on membrane fouling and concluded that viscosity played a secondary role on membrane performance (Moreau et al. (2009)). It is obvious that microfiltration membranes are not able to reject high-molecular viscous solutes as efficiently as ultrafiltration does. Indeed, most of the studies reporting significant effects of MLSS concentration and sludge viscosity on fouling were conducted with microfiltration membranes (Meng et al. (2007); Wang et al. (2006); Wu et al. (2007)). Consequently, distinguishing between the removal efficiency of organic fractions of high molecular weight by ultrafiltration and microfiltration in MBRs would be helpful in order to explain the divergent conclusions drawn regarding the effect of viscosity on fouling in MBRs across the literature.

Contrary to the irrelevant role of sludge viscosity on membrane permeability when the fractions of high molecular weight are efficiently rejected, it was found that viscosity does affect fouling phenomena taking place at the membrane surface. This is evidenced by the change in j_{cr} and $j_{cr,irr}$ observed when treating SWW and HV-SWW. Higher viscosities at the feed side intensify concentration polarization and, thus, gelation of colloids at the membrane surface takes place at low flux levels. In view of these results, investigation of higher and lower aeration intensities at the feed side could provide more information on the relevance of shear-thinning effects on j_{cr} and $j_{cr,irr}$. This question is beyond the scope of the present study although we are confident that our results will motivate further research in this direction. Apart from this, applying backwash has been demonstrated to delay the attainment of critical fouling events also when used with highly viscous fluids. It seems that reversing the flux in intermediate physical cleanings is able to disintegrate gel layers at the initial deposition stages and prevent formation of dense cake layers. Similar results were

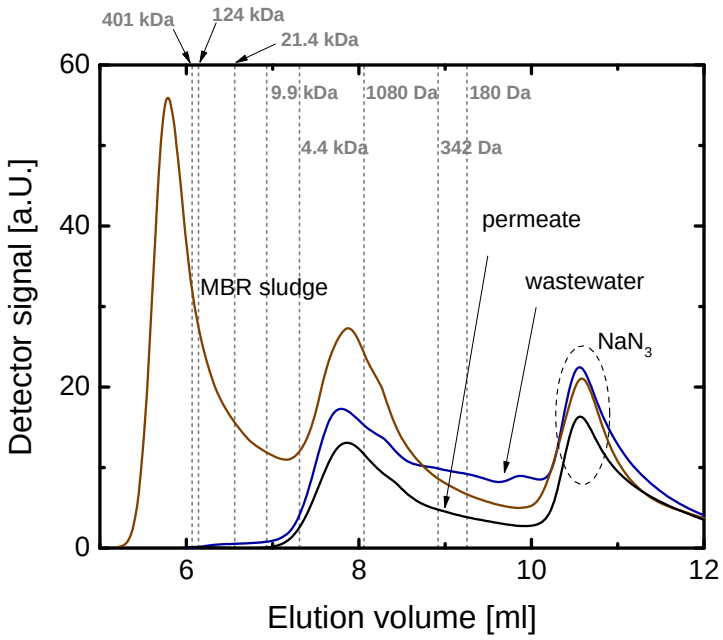

Figure 9: Molecular characterization of the organic fractions present in filtrate samples of MBR activated sludge, MBR feed wastewater and MBR permeate.

also reported by Sabia et al., where backwash was demonstrated to be effective in alleviating fouling associated with cake layer formation on the membrane surface (Sabia et al. (2014)).

5. Conclusions

The interplay between sludge rheology, membrane properties and type of physical cleaning during fouling development in MBRs has been investigated in the present study. The improvement in fouling removal by backwash as compared to relaxation in immersed flat sheet membranes has been demonstrated by comparing the IFSM with the BWSM procedure, which has been developed and presented in this work. The main conclusions of the present paper are summarized as follows:

(i) Backwash has been demonstrated to avoid or delay attainment of critical fluxes. It is efficient already at undercritical fluxes when applied to membranes with a wide pore size distribution. However, backwash does not imply further advantages compared to relaxation for membranes with narrow pores, as internal fouling is not relevant for

these membranes at fluxes below j_{cr}

(ii) In agreement with previous works, $j_{cr,irr}$ exceeds in all cases j_{cr}. This result implies the existence of a range of fluxes above j_{cr} where fouling irreveribility is low, thus extending the range of fluxes where operation of MBRs is sustainable

(iii) High fluid viscosities are strongly related to manifestation of critical fouling at low fluxes. The high shear stress predominating near the membrane surface intensifies concentration polarization, so that gelation or condensation of colloidal matter at the membrane surface occurs at lower fluxes as compared with low-viscous solutions

(iv) As long as critical fouling does not manifest and high molecular weight organic fractions are rejected by the membrane, sludge viscosity does not play a significant role on membrane permeability. On the contrary, membranes with broader pore sizes may suffer from the access into the pores of highly-viscous organic fractions. The increased mass transfer resistance in the pores can easily exceed the resistance of cake layers and concentration polarization, thus decreasing the membrane permeability

All in all, combination of IFSM and BWSM for the investigation of fouling in MBRs has been demonstrated to serve not only to find optimum conditions for operating MBRs but also to improve the understanding about the nature of fouling phenomena and the role of several factors on it. In this respect, the newly introduced BWSM can serve as a useful tool for selection of best membrane during plant design and for optimization of the operation mode during plant operation.

Acknowledgments

M.W. acknowledges the support through an Alexander-von-Humboldt Professorship. M.C. Martí-Calatayud acknowledges the support to Generalitat Valenciana through the funding APOSTD2017. M.C. Martí-Calatayud thanks the contributions of Sybille Hanisch, Sanchita Khandelwal and Sara Vivanco. This work was supported by the German Federal Ministry of Education and Research (BMBF) through the project BRAMAR (02WCL1334A). We thank Synder Filtration for the supplied membranes.

Appendix A. Rheology of permeate samples

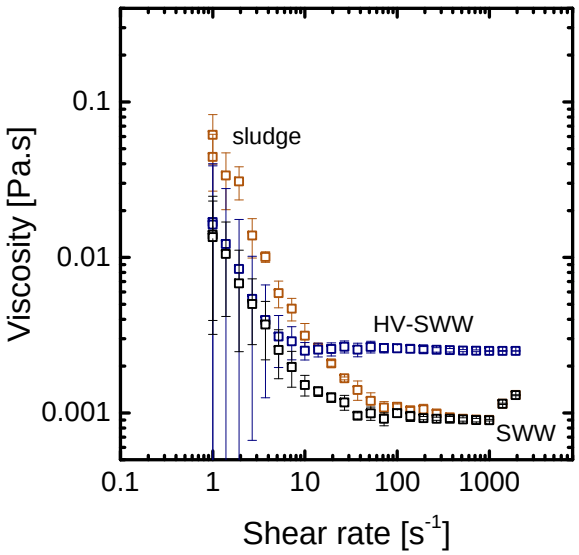

Figure A.10: Rheological behavior of the permeates obtained from filtering the different solutions used in the present study at a temperature of 25° C.

References

Baker, R.W., 2004. Membrane technology and applications. John Wiley & Sons Ltd, Chichester, England. 2nd edition.

Bar-Zeev, E., Passow, U., Romero-Vargas Castrillón, S., Elimelech, M., 2015. Transparent Exopolymer Particles: From Aquatic Environments and Engineered Systems to Membrane Biofouling. Environmental Science & Technology 49, 691–707.

Charcosset, C., Choplin, L., 1995. Concentration by Membrane Ultrafiltration of a Shear Thinning Fluid. Separation Science and Technology 30, 3649–3662.

Cheng, N.S., 2008. Formula for the viscosity of a glycerol-water mixture. Industrial and Engineering Chemistry Research 47, 3285–3288.

Doyen, W., Mues, W., Molenberghs, B., Cobben, B., 2010. Spacer fabric supported flat-sheet membranes: A new era of flat-sheet membrane technology. Desalination 250, 1078–1082.

Drews, A., 2010. Membrane fouling in membrane bioreactorsCharacterisation, contradictions, cause and cures. Journal of Membrane Science 363, 1–28.

Hashino, M., Katagiri, T., Kubota, N., Ohmukai, Y., Maruyama, T., Matsuyama, H., 2011. Effect of surface roughness of hollow fiber membranes with gear-shaped structure on membrane fouling by sodium alginate. Journal of Membrane Science 366, 389–397.

Holloway, R.W., Achilli, A., Cath, T.Y., 2015. The osmotic membrane bioreactor: a critical review. Environ. Sci.: Water Res. Technol. 1, 581–605.

Howell, J., Field, R., Wu, D., 1996. Ultrafiltration of High-Viscosity Solutions : Theoretical Developments and Experimental Findings. Chemical Engineering Science 51, 1405–1415.

Kochkodan, V., Hilal, N., 2015. A comprehensive review on surface modified polymer membranes for biofouling mitigation. Desalination 356, 187–207.

Laera, G., Giordano, C., Pollice, A., Saturno, D., Mininni, G., 2007. Membrane bioreactor sludge rheology at different solid retention times. Water Research 41, 4197–4203.

Le-Clech, P., Chen, V., Fane, T.A., 2006. Fouling in membrane bioreactors used in wastewater treatment. Journal of Membrane Science 284, 17–53.

Lin, H., Zhang, M., Wang, F., Meng, F., Liao, B.Q., Hong, H., Chen, J., Gao, W., 2014. A critical review of extracellular polymeric substances (EPSs) in membrane bioreactors: Characteristics, roles in membrane fouling and control strategies. Journal of Membrane Science 460, 110–125.

van der Marel, P., Zwijnenburg, A., Kemperman, A., Wessling, M., Temmink, H., van der Meer, W., 2009. An improved flux-step method to determine the critical flux and the critical flux for irreversibility in a membrane bioreactor. Journal of Membrane Science 332, 24–29.

Martí-Calatayud, M.C., García-Gabaldón, M., Pérez-Herranz, V., 2013. Effect of the equilibria of multivalent metal sulfates on the transport through cation-exchange membranes at different current regimes. Journal of Membrane Science 443, 181–192.

Martí-Calatayud, M.C., Wessling, M., 2017. Hydraulic impedance spectroscopy tracks colloidal matter accumulation during ultrafiltration. Journal of Membrane Science 535, 294–300.

Meng, F., Chae, S.R., Drews, A., Kraume, M., Shin, H.S., Yang, F., 2009. Recent advances in membrane bioreactors (MBRs): Membrane fouling and membrane material. Water Research 43, 1489–1512.

Meng, F., Shi, B., Yang, F., Zhang, H., 2007. New insights into membrane fouling in submerged membrane bioreactor based on rheology and hydrodynamics concepts. Journal of Membrane Science 302, 87–94.

Meng, F., Zhang, S., Oh, Y., Zhou, Z., Shin, H.S., Chae, S.R., 2017. Fouling in membrane bioreactors: An updated review. Water Research 114, 151–180.

Moreau, A.A., Ratkovich, N., Nopens, I., van der Graaf, J.H.J.M., 2009. The (in)significance of apparent viscosity in full-scale municipal membrane bioreactors. Journal of Membrane Science 340, 249–256.

Pritchard, M., Howell, J.A., Field, R.W., 1995. The ultrafiltration of viscous fluids. Journal of Membrane Science 102, 223–235.

Ratkovich, N., Horn, W., Helmus, F.P., Rosenberger, S., Naessens, W., Nopens, I., Bentzen, T.R., 2013. Activated sludge rheology: A critical review on data collection and modelling. Water Research 47, 463–482.

Rosenberger, S., Helmus, F.P., Drews, A., 2016. Addition of Particles for Fouling Minimization in Membrane Bioreactors - Permeability Performance, Fluid Dynamics, and Rheology. Chemie-Ingenieur-Technik 88, 29–38.

Rosenberger, S., Kubin, K., Kraume, M., 2002. Rheology of Activated Sludge in Membrane Bioreactors. Engineering in Life Sciences 2, 269–275.

Sabia, G., Ferraris, M., Spagni, A., 2014. Online monitoring of MBR fouling by transmembrane pressure and permeability over a long-term experiment. Separation and Purification Technology 122, 297–305.

Wang, Z., Ma, J., Tang, C.Y., Kimura, K., Wang, Q., Han, X., 2014. Membrane cleaning in membrane bioreactors: A review. Journal of Membrane Science 468, 276–307.

Wang, Z., Wu, Z., Yu, G., Liu, J., Zhou, Z., 2006. Relationship between sludge characteristics and membrane flux determination in submerged membrane bioreactors. Journal of Membrane Science 284, 87–94.

Wei, C.H., Huang, X., Ben Aim, R., Yamamoto, K., Amy, G., 2011. Critical flux and chemical cleaning-in-place during the long-term operation of a pilot-scale submerged membrane bioreactor for municipal wastewater treatment. Water Research 45, 863–871.

Wu, Z., Wang, Z., Zhou, Z., Yu, G., Gu, G., 2007. Sludge rheological and physiological characteristics in a pilot-scale submerged membrane bioreactor. Desalination 212, 152–164.

Xing, W., Ngo, H.H., Guo, W., Wu, Z., Nguyen, T.T., Cullum, P., Listowski, A., Yang, N., 2010. Enhancement of the performance of anaerobic fluidized bed bioreactors (AFBBRs) by a new starch based flocculant. Separation and Purification Technology 72, 140–146.

Zhang, H., Gao, Z., Zhang, L., Song, L., 2014. Performance enhancement and fouling mitigation by organic flocculant addition in membrane bioreactor at high salt shock. Bioresource Technology 164, 34–40.

Zhang, M., Peng, W., Chen, J., He, Y., Ding, L., Wang, A., Lin, H., Hong, H., Zhang, Y., Yu, H., 2013. A new insight into membrane fouling mechanism in submerged membrane bioreactor: Osmotic pressure during cake layer filtration. Water Research 47, 2777–2786.

Zsirai, T., Buzatu, P., Aerts, P., Judd, S., 2012. Efficacy of relaxation, backflushing, chemical cleaning and clogging removal for an immersed hollow fibre membrane bioreactor. Water Research 46, 4499–4507.